Carbon Nanodots – Supramolecular Electron Donor-Acceptor Hybrids Featuring Perylenediimides

Volker Strauss[a], Johannes T. Margraf[a,b], Konstantin Dirian[a], XX, XX, Maurizio Prato[c], Andreas Hirsch[a], Timothy Clark[b], Dirk M. Guldi[a]

Affiliations

[a]Department of Chemistry and Pharmacy & Interdisciplinary Center for Molecular Materials (ICMM), Friedrich-Alexander-Universität Erlangen-Nürnberg, Egerlandstr. 3, 91058 Erlangen, Germany

[b]Computer-Chemie-Centrum & Interdisciplinary Center for Molecular Materials (ICMM), Friedrich-Alexander-Universität Erlangen-Nürnberg, Nägelsbachstr. 25, 91058 Erlangen, Germany

[c]Center of Excellence for Nanostructured Materials, Università degli Studi di Trieste, Dipartimento di Scienze Farmaceutiche Piazzale Europa 1, 34127 Trieste, Italy

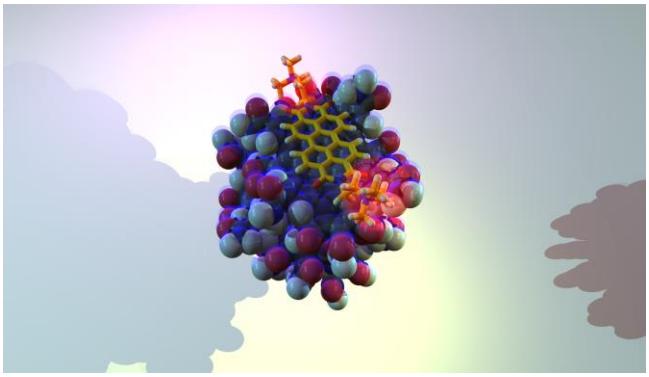

Abstract

We present the formation of charge-transfer complexes that feature electron-donating carbon nanodots (CND) and electron-accepting perylenediimides (PDI). The functionalities of PDIs have been designed to complement those of CNDs in terms of electrostatic and π-stacking interactions based on oppositely charged ionic head groups and extended π-systems, respectively. Importantly, the contributions from electrostatic interactions were confirmed in reference experiments with PDIs that feature negatively rather than positively charged head groups. The electronic interactions between the components in ground and excited state were characterized in complementary absorption and fluorescence titration assays that suggest charge-transfer interactions in both states with binding constants on the order of 8×10^4 M^{-1} (25 L g^{-1}). Our investigations were rounded off by selective excitation of the two components in ultrafast pump probe experiments leading to the formation of a 210 ps lived charge separated state.

Introduction

Carbon is the key to many technological applications, from drugs to synthetic materials, that have become indispensable in our daily life and have influenced the world's civilization for centuries.[1] Importantly, the structural diversity of organic compounds and molecules results in sheer endless chemical and physical properties.[2,3] Altering the periodic binding motifs in networks of sp^3-, sp^2-, and *sp*-hybridized C-atoms represents the conceptual starting point for constructing a wide palette of carbon allotropes.[4] To this end, the past two decades have served as a test-bed for measuring the physico-chemical properties of carbon in reduced dimensions starting with the advent of *fullerenes (0D)*, followed in chronological order by *carbon nanotubes (1D)*, *graphene (2D)* and recently *carbon nanodots (2D)*. These species are now poised for use in wide-ranging applications.[5]

The design of new, simple, and inexpensive photosensitizers is important, especially in the conversion of solar energy for emerging areas such as light harvesting, energy storage, and sensors.[2,6–8,9] In this context, exploring novel carbon materials based on light-absorbing and/or -emitting charge-transfer states is expected to play a key role.[10] One versatile strategy *en route* to charge-transfer states is to combine molecular building blocks that are complementary in terms of electronic levels and binding motifs.[11–14] In this context, carbon nanodots (CND) represent a well-known class of molecular materials that has recently shown great promise for solar energy conversion. CNDs are strong light emitters that feature broad and, more importantly, tunable absorptions throughout the visible range of the solar spectrum.[15] The basis for a comprehensive understanding of the CNDs' photophysical properties has been laid out in a number of combined experimental and/or theoretical studies.[16]

Both bottom-up approaches and top-down approaches to the synthesis of CNDs have been described in recent years. Thermal or microwave-assisted and electrochemical deposition syntheses are prominent examples for bottom-up approaches, while synthetic strategies such as the oxidation of graphite and cage opening of fullerenes typify top-down strategies.[17,18,19] Whatever the synthesis route, the sizes of CNDs typically range from 1 to 10 nm with different numbers of stacked graphene layers that are saturated with functional groups at their periphery. Importantly, their facile synthesis and low cost make CNDs promising replacements for expensive organic dyes in optoelectronic applications.[17,20–22,23,24]

The charge-transfer activity of CNDs has recently been explored, both in the ground and in the excited states,[25,23] the latter in conjunction with a variety of electron donors and acceptors.[26,22] For instance, CNDs have been used together with complementary forms of nanocarbons such as fullerenes, carbon nanotubes, graphene, etc. in tailored charge-transfer systems. In a leading example, CNDs have been

combined with single-walled carbon nanotubes (SWCNTs) affording supramolecular nanohybrids, in which the components function as electron donors and acceptors, respectively.[27] Graphene-oxide/CND nanohybrids have also been found to feature remarkable charge-transfer activity.[23]

We recently reported a novel synthetic approach that gives uniform ~1 nm CNDs.[22] Moreover, we demonstrated that CNDs form stable charge-transfer hybrids with either electron donors or acceptors. The mutual electron donor-acceptor interactions can be fine-tuned using electrostatic interactions with the negatively charged edge groups of CNDs. Furthermore, the central units of the CND layers feature extended π-systems, which is susceptible for π-stacking interactions.

Perylenediimides (PDI) can complement CNDs in order to form charge-transfer complexes because they are strong electron acceptors and also feature an extended π-system.[28,29] One great advantage of PDIs is their broad range of possible functionalization, which allows their structural and electronic properties to be tailored.[30,31] For instance, PDIs are easily functionalized with positively or negatively charged head groups at the imido positions.[32] We show below that functionalization with positively charged ammonium head groups is critical for stable interactions with negatively charged CNDs. Interactions between CNDs and PDIs in the ground state have been investigated using voltammetry and steady-state absorption spectroscopy. As a complement, excited-state dynamics and reactions have been investigated using both steady-state and time-resolved emission spectroscopy and ultrafast pump-probe experiments. Density-functional theory (DFT) and configuration-interaction calculations based on semiempirical molecular-orbital theory have been used to help clarify the experimental results.

Results and Discussion

Characterization of the individual components

PDIs **1** and **2** were synthesized using a published procedure.[32] PDIs **1** and **2** have identical PDI cores, but positive and negatively charged head groups, respectively, at their imido positions (see Figure 1). **1** is substituted with two positively charged trimethylammonium groups, while **2** bears first-generation, negatively charged Newkome-type dendrons. The following discussion will focus on the experimental results found for **1**, the reference experiments with **2** are described in the Supporting Information.

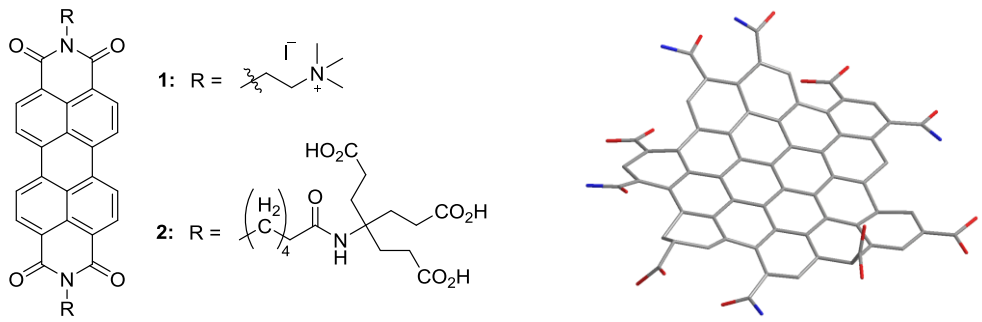

*Figure 1. Molecular structures of PDI **1** and **2** (left) and a representative structure of pCND (right).*

Figure 2 shows the absorption spectrum of **1**, which resembles the typical PDI absorption pattern with maxima at 500 and 533 nm and a shoulder at 470 nm with extinction coefficients as high as 3.0×10^4 $M^{-1}cm^{-1}$.[33] The vibrational splitting seen for **1** with the 500 nm peak being stronger than the one at 533 nm, indicates PDI aggregation.[33] Two well defined maxima at 545 and 587 nm with an intensity ratio of 2.5:1 are found in the fluorescence spectrum of **1**. The fluorescence quantum yields were determined to be 5.9%, from which we conclude that the fluorescence originates from monomeric rather than aggregated PDIs, in line with the fluorescence lifetime measurements, in which only a single lifetime of 4.7 ns was found.

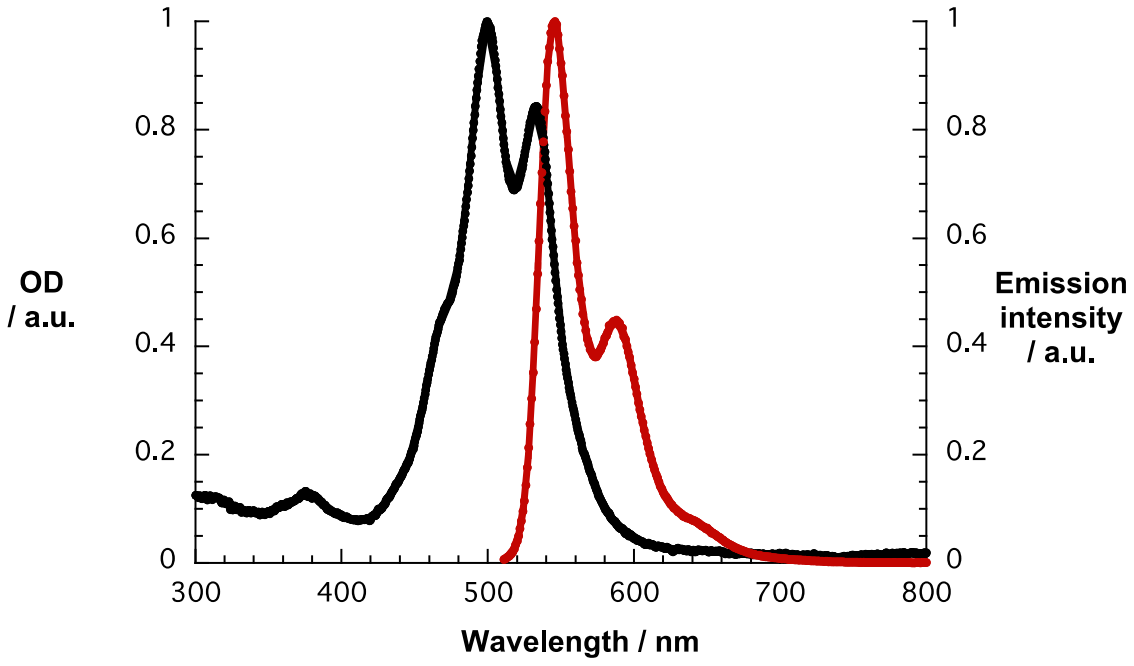

*Figure 2. Normalized absorption (black spectrum, c = 1 × 10^{-5} M) and fluorescence (red spectrum, λ_{ex} = 500 nm, c = 1 × 10^{-5} M) spectra of **1** in D_2O.*

The absorption and fluorescence spectra of **2** (shown in Figure S1) show similar, but slightly red-shifted characteristics. For example, the absorption maxima occur at 500 and 540 nm and the intensity of the long wavelength maximum is notably weaker than for **1**. The maxima in the fluorescence spectra appear at 548 and 589 nm with an intensity ratio that, again, indicates that monomeric PDIs are the origin of the fluorescence. The extinction coefficient and fluorescence quantum yield, 2.7 × 10^4 $M^{-1}cm^{-1}$ and 5.5%, respectively, of **2** are close to those found for **1**.

The pCNDs were produced under mild reaction conditions in a microwave reactor (see experimental section).[34,22] The absorption spectrum, which is shown in Figure 3, shows a prominent maximum at 339 nm, a shoulder at around 410 nm, and a weak absorption tail reaching into the visible part of the spectrum. The fluorescence spectrum found upon excitation at 350 nm is best described as a broad peak with its maximum at 443 nm. Notably, the pCND fluorescence is biphasic; photoexcitation at 500 nm results in weak features with a maximum at 592 nm, as shown in Figure 3.

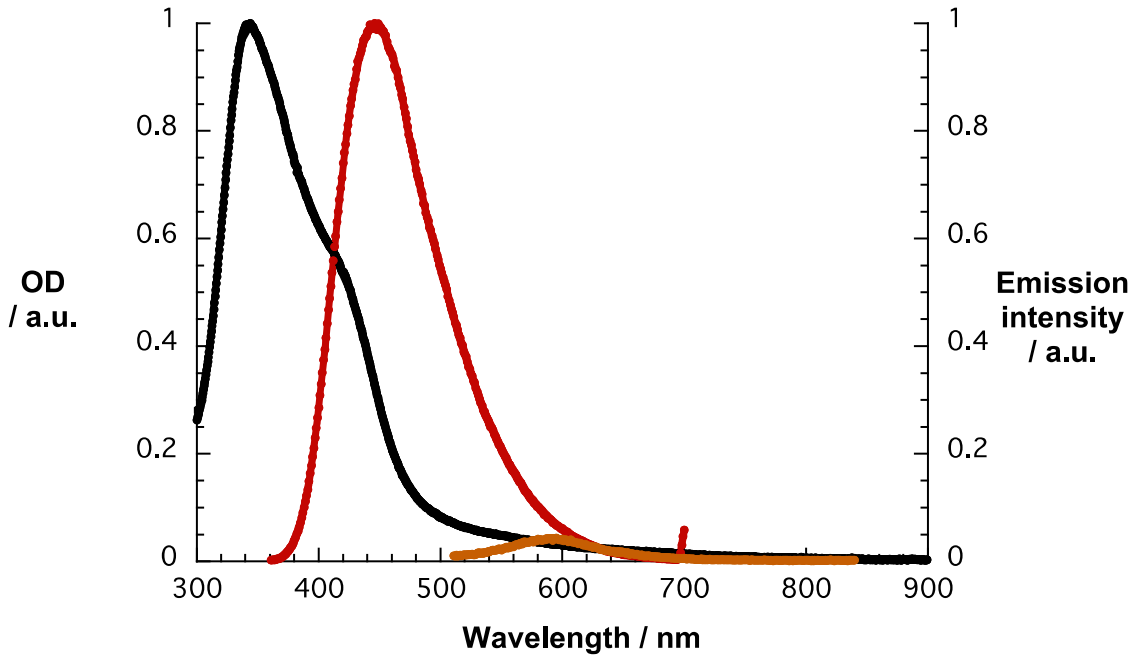

Figure 3. Normalized absorption (black spectrum, c = 1 × 10^{-5} M) and fluorescence (λ_{ex} = 350nm, red spectrum, and 500

nm, orange spectrum) spectra of pCND in D_2O.

Electrochemical Characterization

The electrochemical characterization was performed using cyclic voltammetry and differential pulse voltammetry. The voltammograms of **1** and pCND, measured against an Ag/AgCl reference electrode, are shown in Figure 4. Neither cyclic nor differential pulse voltammograms of pCND reveal appreciable signals in the reductive voltage region up to -0.8V in aqueous solution. In stark contrast, **1** shows two reduction waves at -0.5 V and -0.72 V, which we assign to the first and second reductions of **1**, respectively. The re-oxidations occur at -0.34 and -0.27 V in the reverse scan direction. The voltammograms of **2** are shown in Figure S2 of the Supporting Information. No distinct reductions of **2** were discernable in aqueous solution. The first reduction of **2** was detected in methanol -0.35 V vs. Ag/AgCl.

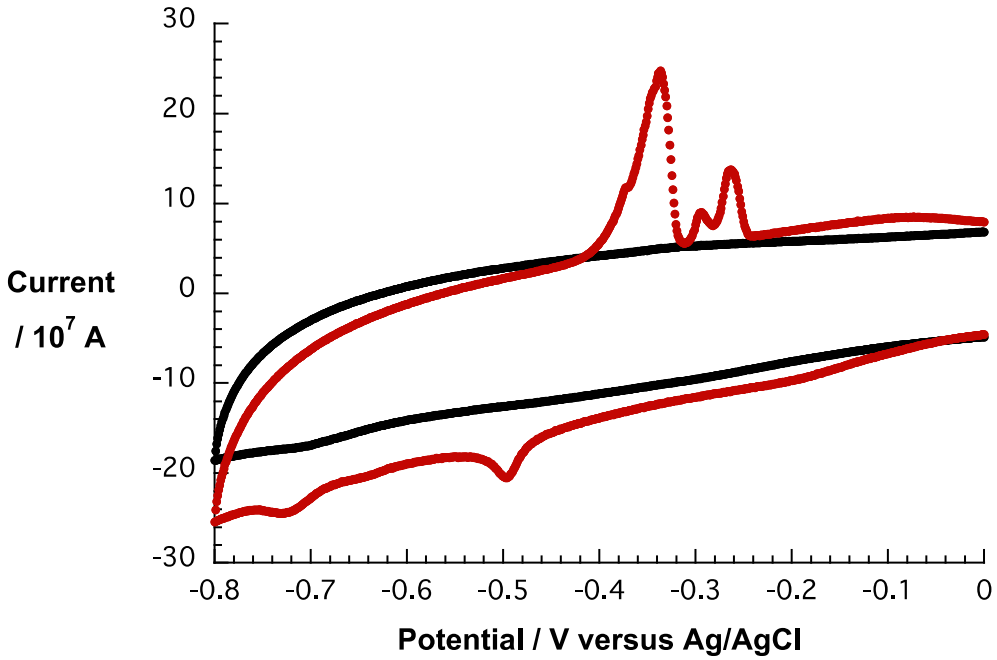

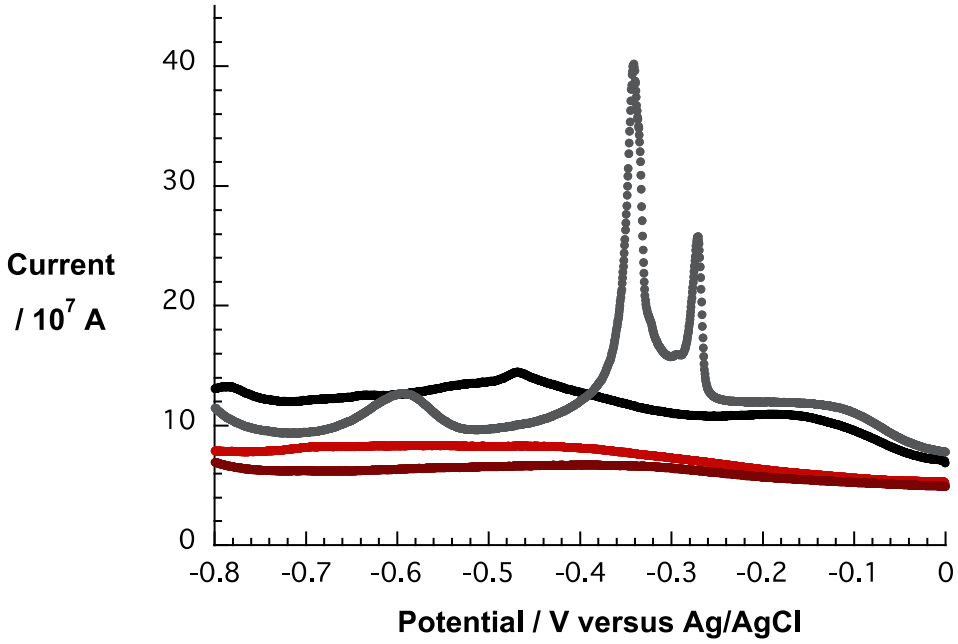

*Figure 4. Cyclic voltammograms (above) and differential pulse voltammograms (below) of **1** (red spectrum) and pCND (black spectrum) in D_2O with NaCl as supporting electrolyte (negative scan direction: black spectrum and red spectrum, positive scan direction: grey spectrum and wine spectrum)*

Complexation – Photophysical Characterization

Steady state absorption titration assays provided information about the non-covalent assembly of pCND with **1**. The concentration of **1** was kept constant, pCND added sequentially and the absorption changes monitored. The results are shown in Figure 5. A significant decrease of the PDI-centered absorptions between 450 and 600 nm down to 67% of the original intensity is observed with increasing concentrations of pCND. This is a typical indicator for the non-covalent complexation of pCND and **1** to afford pCND/**1.**[35] Moreover, a shift of the absorption maxima from 500 and 535 nm to 502 and 539 nm, respectively, suggests significant electronic communication between pCND and **1**. In contrast, the lack of changes for PDI-centered absorptions in the corresponding titrations of **2** with pCND up to a concentration of 0.1 g L^{-1} indicates neither complexation nor ground-state interactions, as shown in Figure S4 of the Supporting Information.

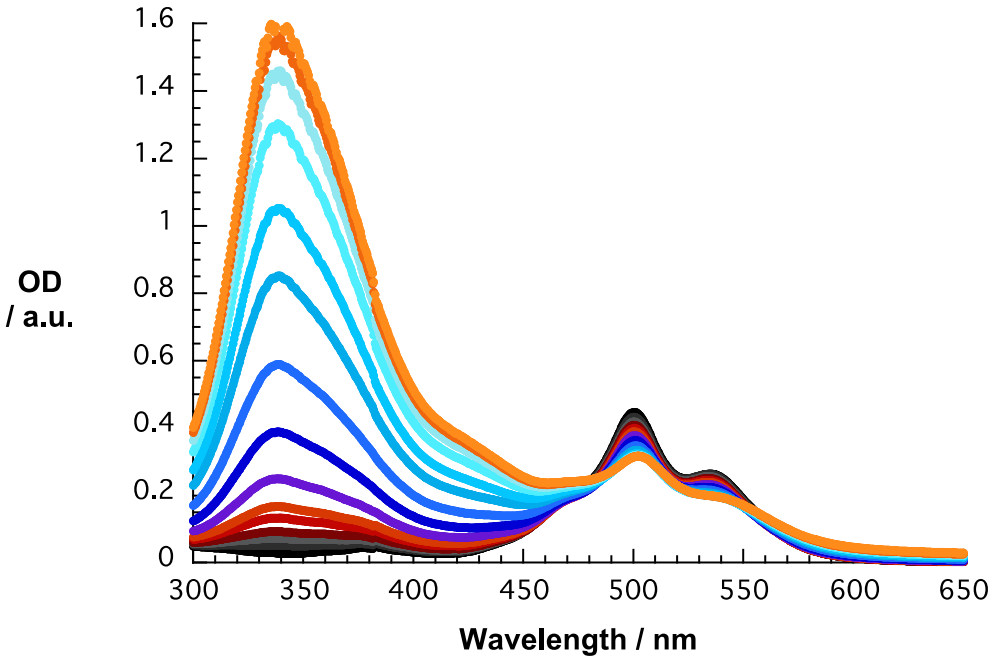

*Figure 5. Absorption spectra of **1** (orange spectrum, 10^{-5} M) during the course of a titration with pCND (blue>red>black spectra, 0-0.1 g L^{-1}) in phosphate-buffered D_2O (pH=7.2) at room temperature.*

1 can be excited selectively at 500 nm. Addition of pCND to **1** leads to an exponential quenching of the PDI-centered fluorescence. This is reflected in the Stern-Volmer plot shown in Figure 6, which indicates a binding constant of 25 L g^{-1}. Finally, the fluorescence decay in the resulting pCND/**1** is best fit by a two-exponential decay function with lifetimes of 0.3 and 4.7 ns with a relative weight distribution of 0.15 to 0.85. In analogous titration experiments with **2** and variable pCND concentrations, only a very weak fluorescence quenching is discernable, as shown in Figure S5 of the Supporting Information.

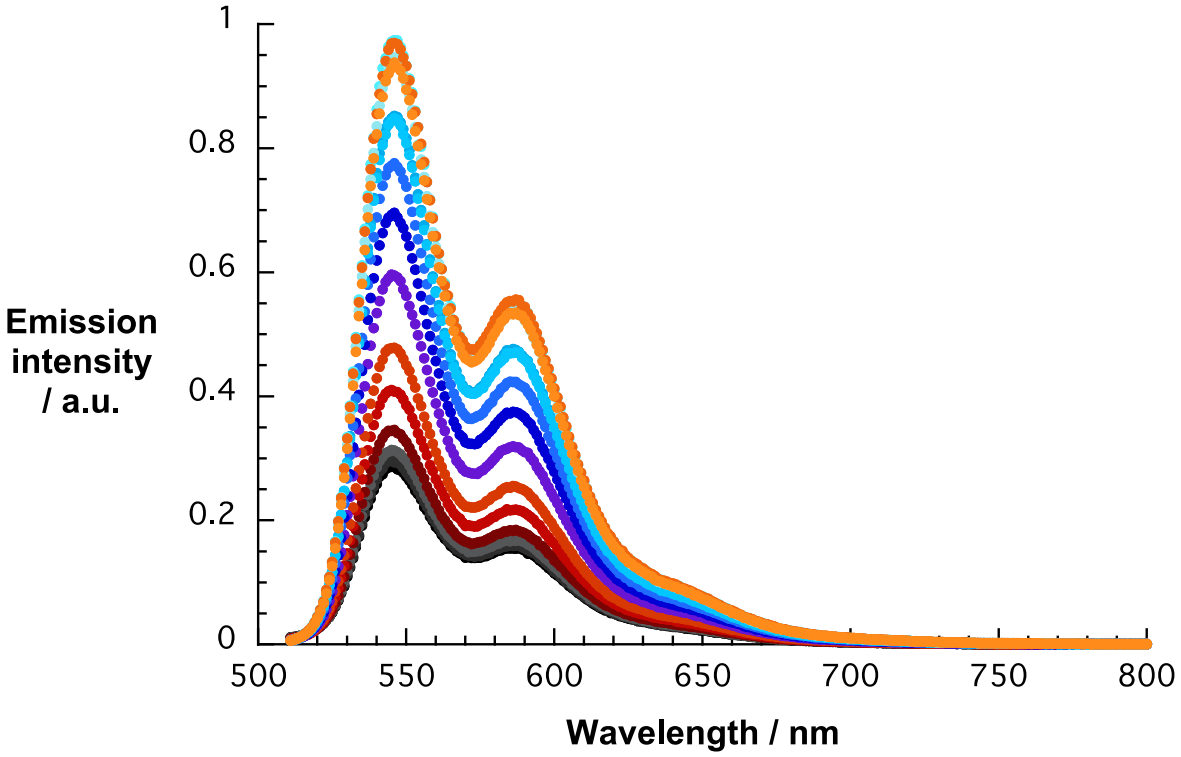
Emission intensity / a.u.
1
0.8
0.6
0.4
0.2
0
500
550
600
650
700
750
800
Wavelength / nm

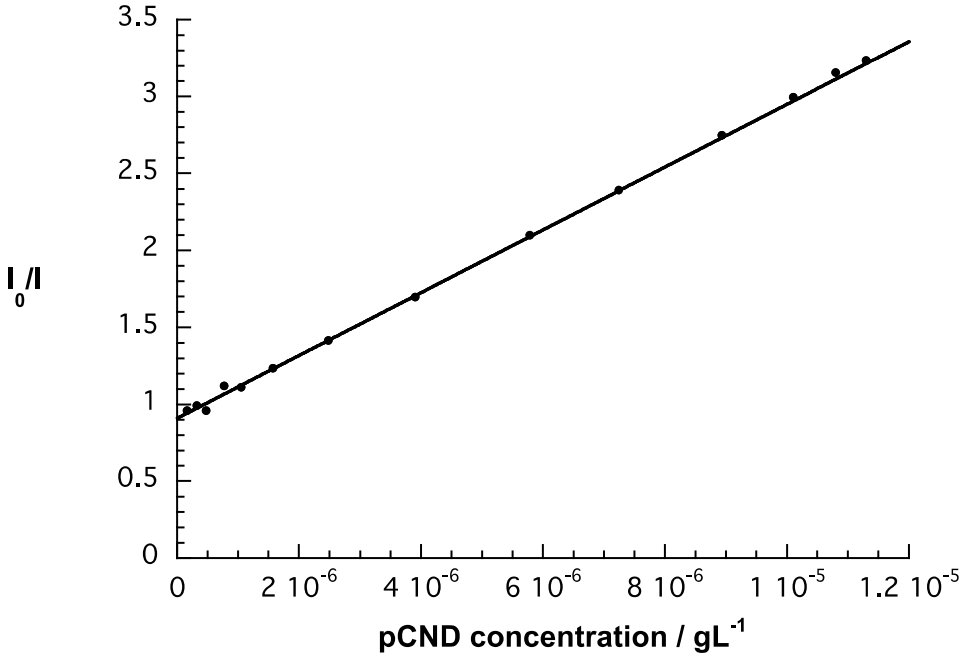
I0/I
3.5
3
2.5
2
1.5
1
0.5
0
0
2 10-6
4 10-6
6 10-6
8 10-6
1 10-5
1.2 10-5
pCND concentration / gL-1

*Figure 6. Above: fluorescence spectra of **1** (black spectrum, 10^{-5} M) during the course of a titration with pCND (red>blue>orange spectra, 0-0.1 g L^{-1}**)** in phosphate-buffered D_2O (pH=7.2) at room temperature. Below: relationship of I/I_0 versus the concentration of pCND used to determine the association constant.*

To analyze the photophysical changes of pCND further, reversed titrations using a constant concentration of pCND and variable amounts of **1** were conducted. The most striking observation in the absorption titration assays is the strong decrease in pCND centered absorptions shown in Figure 7. Again, a change in absorption is a reliable indicator of electronic interactions between pCND and **1**. A careful analysis of the pCND absorption features reveals a concentration-dependent blue shift from 339 to 337 nm and formation of a 375 nm shoulder. In line with the evidence discussed above, pCND and **2** show no evidence of interactions (Figure S6 of the Supporting Information).

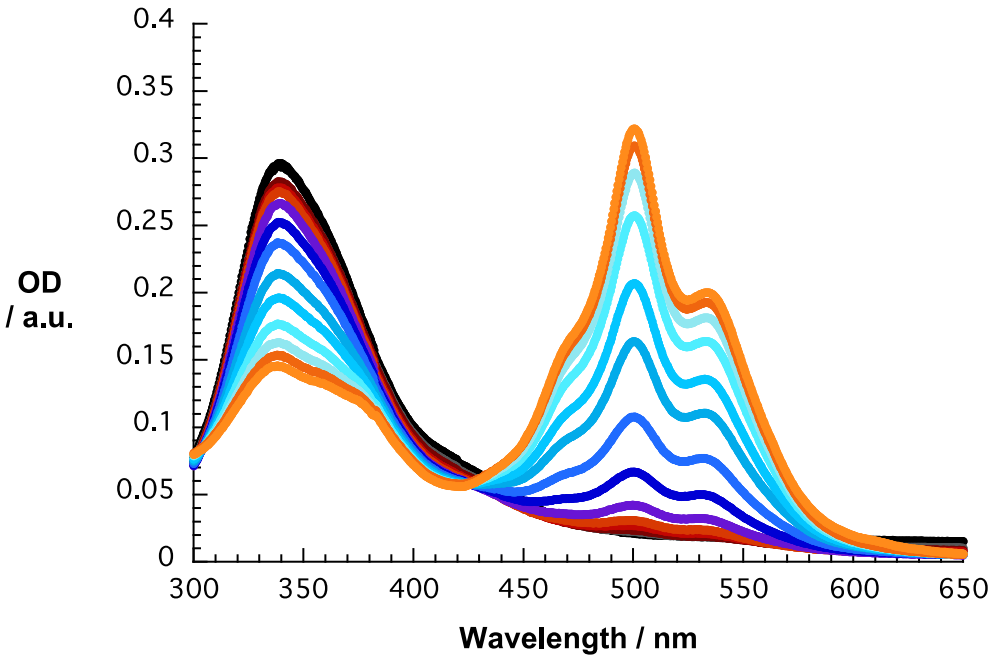

*Figure 7. Absorption spectra of pCND (black, 0.2 g L^{-1}) (black spectrum) during the course of a titration with **1** (red>blue>orange spectra, 0-1×10^{-5} M**)** in phosphate-buffered D_2O (pH=7.2) at room temperature.*

Steady state fluorescence assays indicate that the addition of **1** causes strong quenching. Note that 350 nm radiation excites both components, so that pCND and **1** both fluoresce, which was taken into account during the quantitative analyses. Figure 8 shows the Stern-Volmer plot obtained, which deviates to higher values than expected from a linear dependence at higher concentrations of **1**. This deviation suggests that, in addition to static quenching in pCND/**1** with a binding constant of 8.0×10^4 M^{-1}, collisional quenching between pCND and **1** is operative. As in the absorption assays, a

considerable blue shift of the fluorescence from 443 to 439 nm and a narrowing is found, as shown in Figure 8. Once again, spectral changes found in the titration assays between pCND and **2**, are barely detectable, as shown in Figure S7 of the Supporting Information.

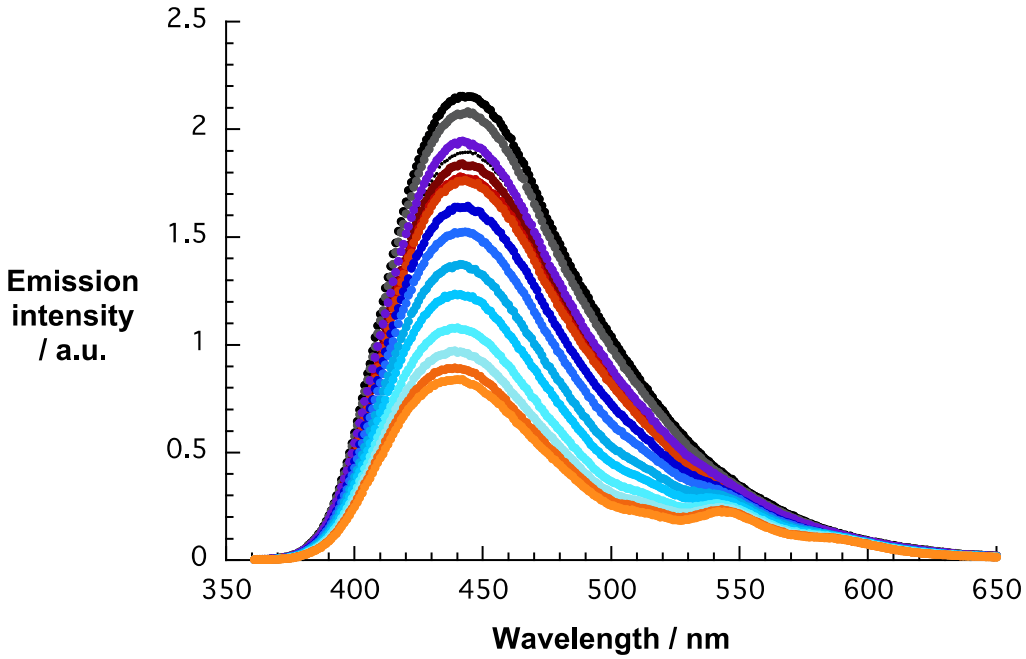

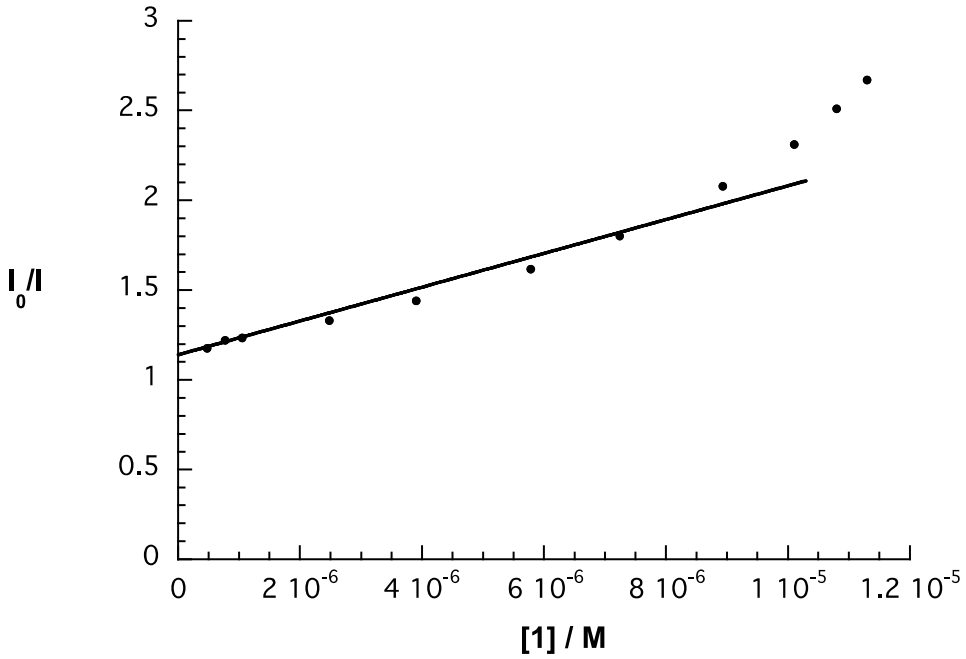

*Figure 8. Above; fluorescence spectra of pCND (black spectrum, 0.2 g L^{-1}) during the course of a titration with **1** (red>blue>orange spectra, 1-10^{-5} M**)** in phosphate-buffered D_2O (pH=7.2) at room temperature. Below; relationship of I/I_0 to the concentration of **1** used to determine the association constant.*

The role of the ionic interactions as a binding motif between **1** and pCND was investigated by steadily increasing the ionic strength of the solution by adding potassium chloride. In unbuffered solution, a fluorescence quenching of 15 % compared to pure **1** was found for pCND/**1**. Upon addition of KCl, the fluorescence recovered partially to a value of 23 %, as shown in Figure S8 of the Supporting Information. A blue-shift of the maxima – shown in Figure S9 of the Supporting Information – is found in the absorption spectra of the complex. However, neither the extinction nor the fluorescence of **1** recovered fully.

To obtain further information about ground-state interactions between pCND and **1**, we recorded voltammograms of different mixtures of pCND and **1**. Note that oxidation signals of pCND can be only detected in polar organic solvents such as MeOH or DMSO and appear in the positive voltage region between 0.6 and 1.2 V. Because of this, we focused on the cathodic scans, in which only the one-electron reduction of **1** takes place. Figure 9 shows a significant shift of the one-electron reduction of **1** towards more negative potentials upon addition of pCND. This implies a shift of electron density from the electron donating pCNDs to **1** that renders the reduction of the latter more difficult. Plots of

the shift in the reduction potential versus the pCND concentration show a clear exponential dependence that corresponds to a binding constant of ~50 g L^{-1}.

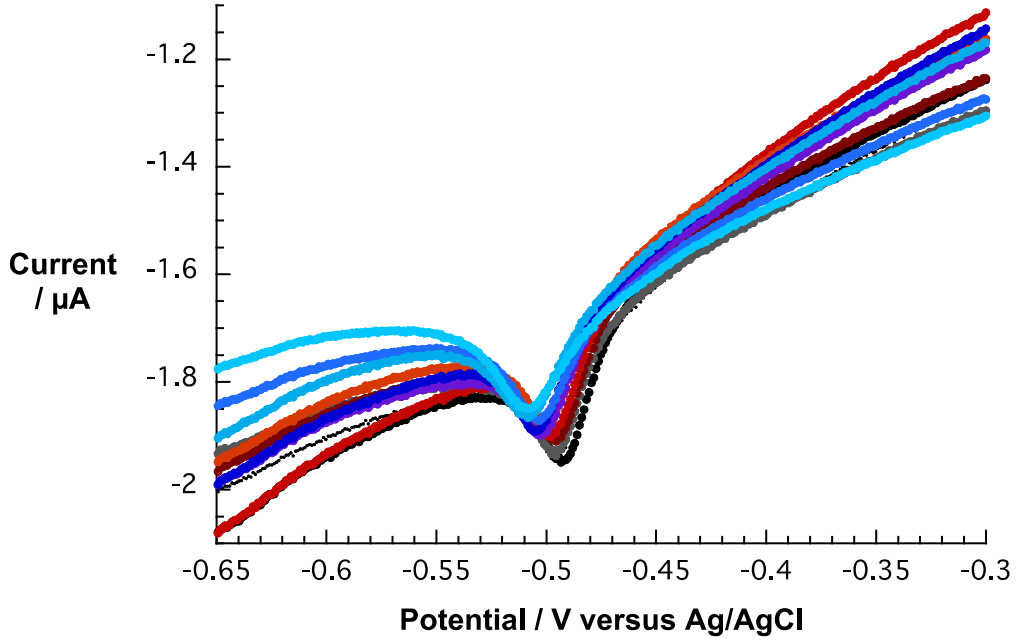

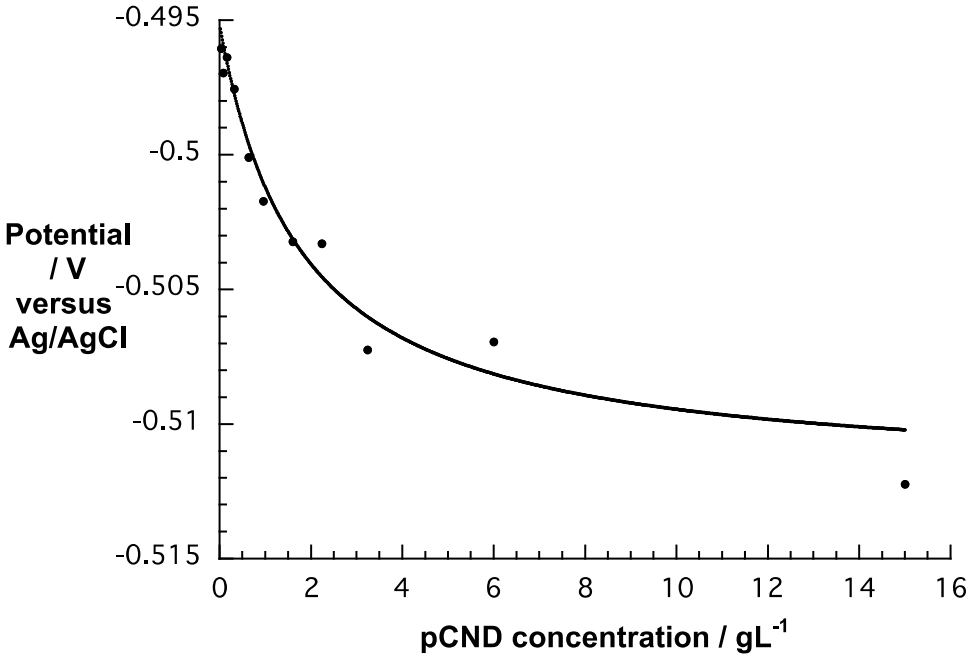

*Figure 9. Above; reductive scans of cyclic voltammograms of **1** (black spectrum, 6×10^{-4} M (0.5 g L^{-1})) during the course of a titration with pCND (red>blue spectra, 0-15 g/L) in H_2O with NaCl as supporting electrolyte. Below; peak potential versus the concentration of pCND that was used to determine the association constant.*

Calculations

Density-Functional Theory (DFT) calculations at the PBE+D/DNP level with the dispersion correction of Tkatchenko and Scheffler[29-31] were used to help elucidate the nature of the interaction between **1** and pCNDs. Water solvation was considered implicitly using the COSMO model.[32] All calculations were performed with dMol3.[33,34] As in our previous work on pCNDs, we based the models on heavily functionalized graphene fragments. In this case, we added two carboxylate groups to form neutral complexes with **1**. We used three pCND models, which differed only in the location of the carboxylate groups leading to different complexes, as shown in Figure 10.

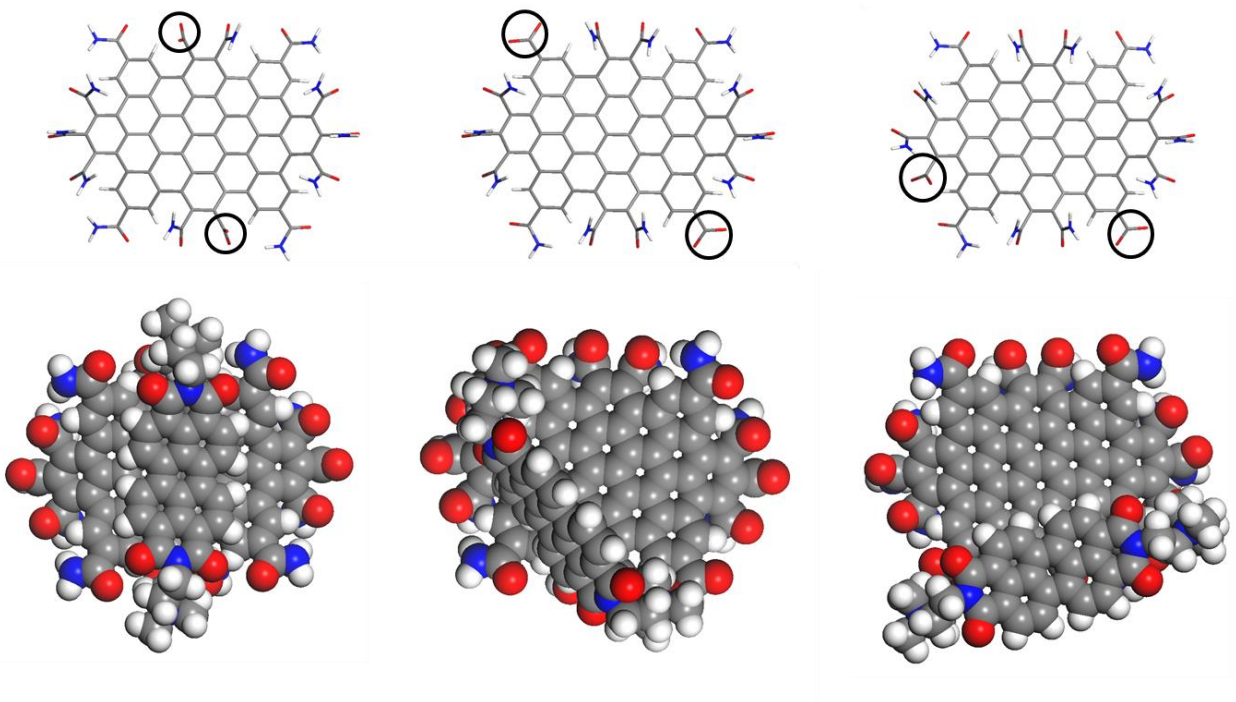

*Figure 10. Above; structures of the pCND models, the carboxylate groups are marked with black circles. Below; pCND/**1** complexes referred to as top (left), diagonal (center) and side (left), according to the orientation of **1** relative to pCND.*

The complexes are formed either mainly through ionic interactions between the ammonium and carboxylate groups (*diagonal* and *side* geometry) or through mixed ionic/π-π interactions (in the *top* geometry). The *top* geometry is energetically favored, with an interaction energy of -51.3 kcal mol^{-1} compared to -30.5 and -26.6 kcal mol^{-1} for the *diagonal* and *side* geometries, respectively. However, our pCND model is somewhat idealized; the formation of mixed ionic/π-π complexes may be hindered by greater steric repulsion in the real case.

We then performed semiempirical configuration interaction with single excitations (CIS) calculations on these systems in order to understand the effect of the complex orientation on the nature of the pCND/**1** charge-transfer state. These calculations were performed with VAMP using the PM6 Hamiltonian.[35,36] The calculations reproduced the experimental UV/Vis spectrum of **1** quite well, as shown in Figure S10 of the Supporting Information. The lowest energy charge-transfer state shows charge shift from the pCND to **1** in all cases, as shown in Figure 11. The excitation energies show a similar dependence on the complex geometry to the interaction energies. The calculated vertical excitation energies are 2.9 eV for the *top* orientation, 4.0 and 3.8 eV for the *diagonal* and *side* orientations, respectively.

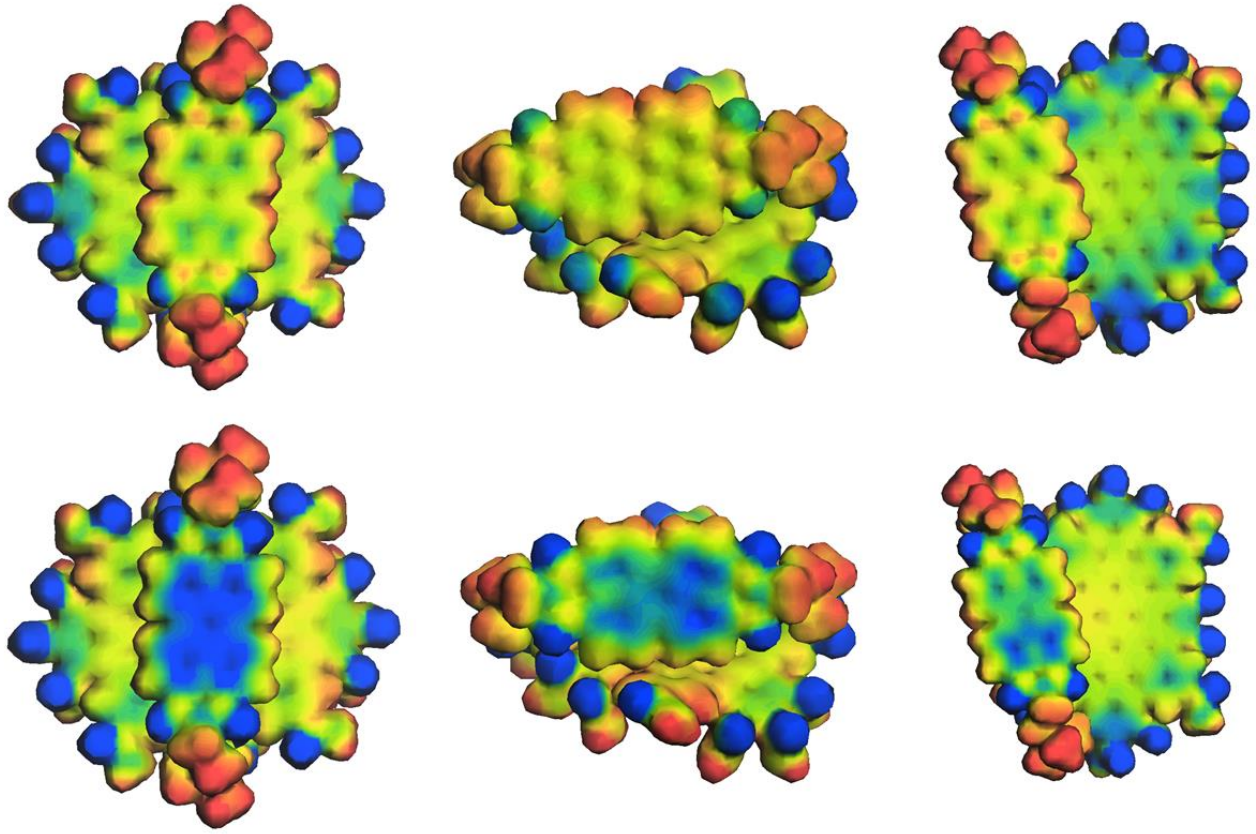

*Figure 11. Above; ground-state molecular electrostatic potentials of pCND/**1** complexes. Below; molecular electrostatic potentials of the respective lowest energy charge transfer states. Color code from -0.2 (blue) to 0.2 (red) Ha e^{-1}.*

We conclude that photoinduced charge separation is a likely cause for the emission quenching observed in pCND/PDI complexes, independent of the binding motive. The spatial contact between the π-systems in the *top* geometry stabilizes the charge-separated state.

Excited-State Dynamics

Fluorescence lifetime measurements using time-correlated single-photon counting (TCSPC) showed the addition of pCND to exert considerable impact on the excited-state lifetimes of **1**, as shown in Figure S11 of the Supporting Information. In the absence of pCND, the singlet excited state decays mono-exponentially with a lifetime of 4.7 ns. In the presence of pCND, two lifetimes of 4.7 and 0.2 ns were found. Note that the mass ratio of pCND to **1** was less than 1:5 to avoid full quenching of the fluorescence of **1**. We assign the long lifetime of 4.7 ns to free, uncomplexed **1** and the 0.2 ns lifetime to a deactivation in pCND/**1** through energy or electron transfer. Complementary lifetime measurements showed that the lifetimes of **2** remained unchanged upon addition of pCND in a concentration regime of up to 0.05 g L^{-1}, as shown in Figure S12 of the Supporting Information.

Femtosecond transient-absorption measurements following excitation at either 387 or at 500 nm allowed selective excitation of pCND or **1** / **2**, respectively. For **1**, 500 nm excitation leads to the instantaneous formation of a strong minimum at 498 nm and several maxima at 543, 590, 735, and 963 nm, as shown in Figure 12. The minimum represents the ground-state bleaching as it is the inverse of the absorption spectrum. We assign the positive transients ranging from 543 to 1200 nm to excited-state absorptions. Multi-wavelength lifetime analyses yield two dominant components of 150 and 300 ps. Figure S13 of the Supporting Information shows that the pump probe experiments with **2** exhibited similar deactivation behavior. Lifetimes of 20 and 330 ps underline, once again, the resemblance to the electronic structure of **1**.

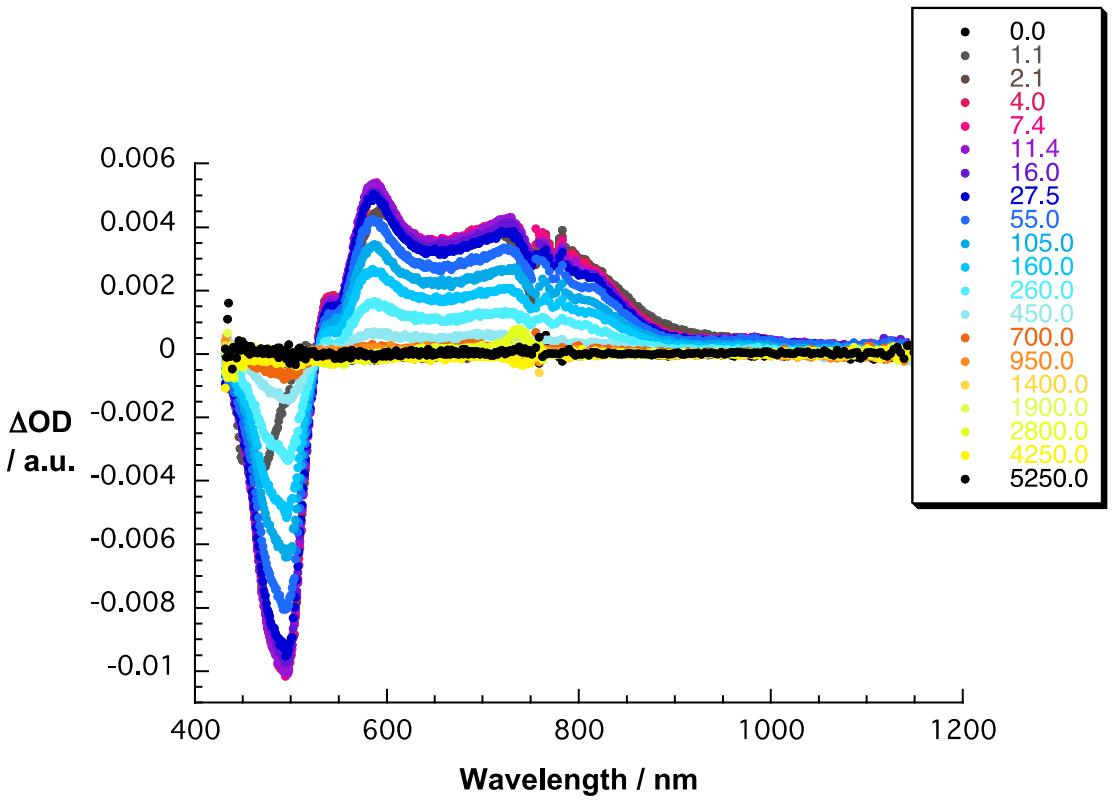
0.0
1.1
2.1
4.0
7.4
11.4
16.0
27.5
55.0
105.0
160.0
260.0
450.0
700.0
950.0
1400.0
1900.0
2800.0
4250.0
5250.0
0.006
0.004
0.002
0
-0.002
-0.004
-0.006
-0.008
-0.01
ΔOD
/ a.u.
400
600
800
1000
1200
Wavelength / nm

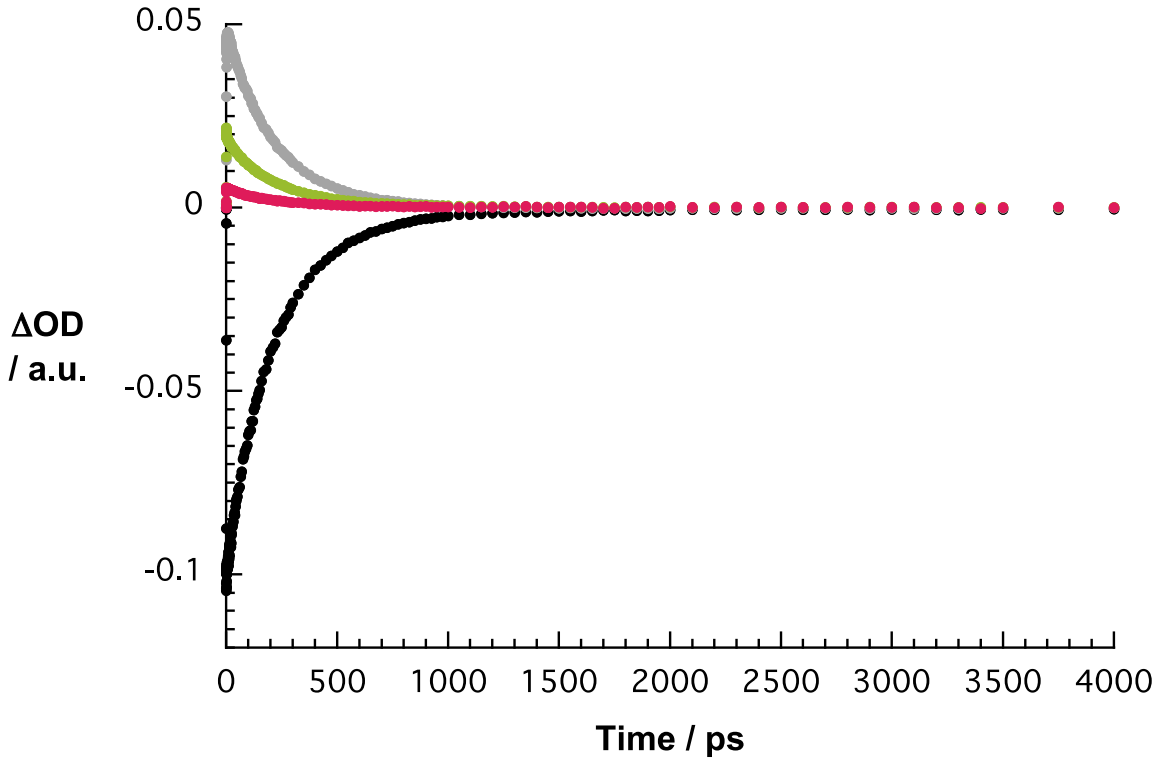

*Figure 12. Above; differential absorption spectra obtained upon femtosecond pump probe experiments (500 nm) of **1** (1 × 10^{-5} M) in phosphate-buffered D_2O (pH=7.2) with several time delays in ps between 0 and 5250 ps (grey>blue>yellow>black spectra) at room temperature. Below; time absorption profiles of the spectra shown in the above at 500 nm (black spectrum), 591 nm (grey spectrum), 850 nm (green spectrum), and 1000 nm (magenta spectrum) monitoring the singlet excited state decay.*

Typical features of reduced **1** at 703, 825, and 990 nm are found in corresponding femtosecond transient absorption measurements with pCND/**1**, as shown in Figure 13. Moreover, the ground-state bleaching at 500 nm is significantly weaker. Furthermore, the presence of pCND impacts the lifetime of the transient absorptions strongly. A global fitting of the transient absorptions yielded a short lifetime of 4 ps and a longer one of 210 ps. The long-lived component does not vary at different concentrations of pCND. Therefore, it is safe to assign the long component to anion-related features. Consistent with the observations from the steady state spectrophotometric and voltammetric titrations, the immediate formation of the anion-related signatures points to instantaneous complex formation. Analogous behavior was seen upon excitation at 387 nm (Figures S15 and S16 of the Supporting Information). However, strong superimpositions with the excited-state absorptions of pCND dominate the spectra. No anion-related signals were detected in the reference experiments with **2** and pCND (Figure S14 of

the Supporting Information); the excited-state absorption pattern of **2** remains unchanged upon addition of different amounts of pCND. Moreover, a multi-wavelength lifetime analysis confirms that the presence of pCNDs does not affect the excited-state deactivation of **2**.

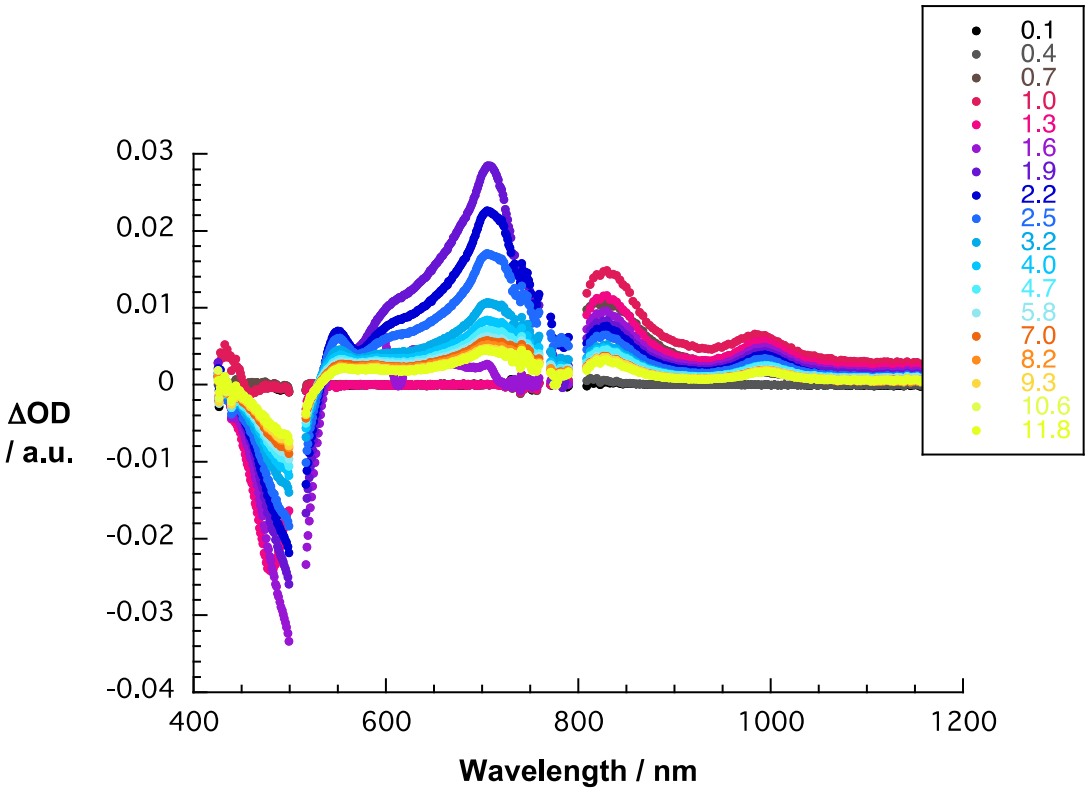
0.1
0.4
0.7
1.0
1.3
1.6
1.9
2.2
2.5
3.2
4.0
4.7
5.8
7.0
8.2
9.3
10.6
11.8
0.03
0.02
0.01
0
-0.01
-0.02
-0.03
-0.04
ΔOD
/ a.u.
400
600
800
1000
1200
Wavelength / nm

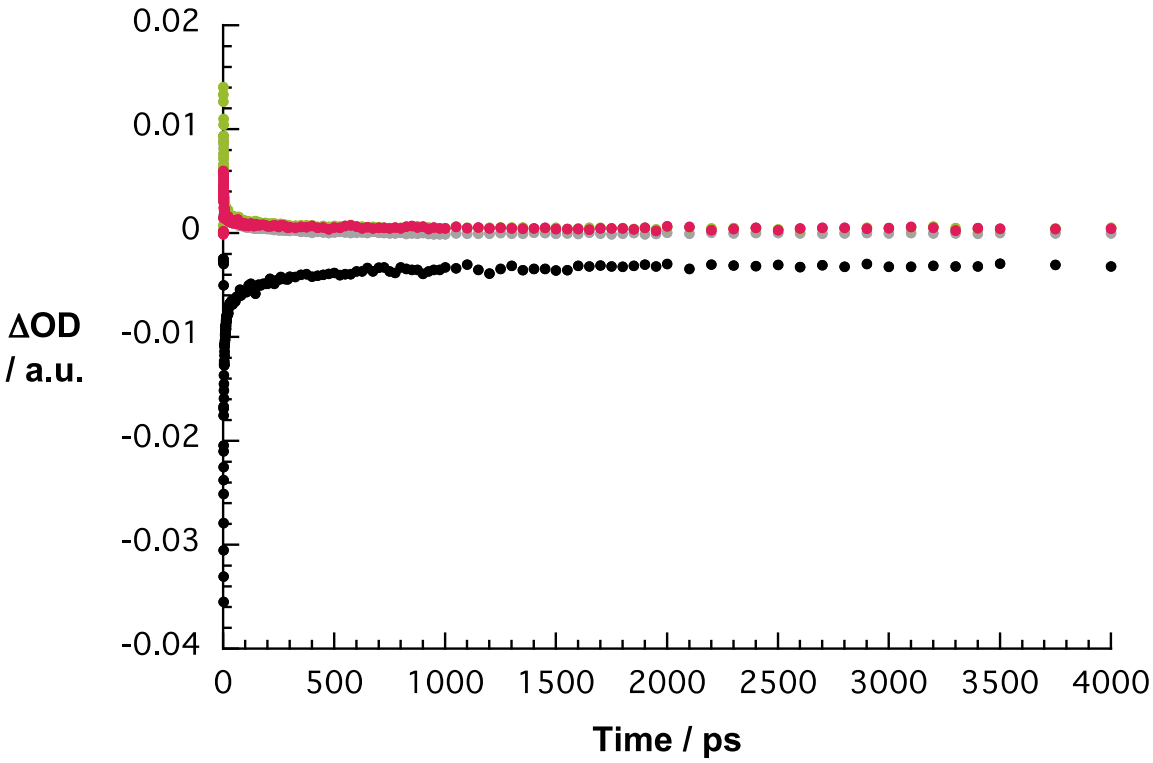
0.02
0.01
0
-0.01
-0.02
-0.03
-0.04
ΔOD
/ a.u.
0
500
1000
1500
2000
2500
3000
3500
4000
Time / ps

*Figure 13. Above; differential absorption spectra obtained upon femtosecond pump probe experiments (500 nm) of pCND/**1** (1 × 10^{-5} M**)** in phosphate-buffered D_2O (pH=7.2) with several time delays in ps between 0 and 12 ps (grey>rot>blau>orange>yellow spectra) at room temperature. Below; time absorption profiles of the spectra shown in the above at 500 nm (black spectrum), 591 nm (grey spectrum), 850 nm (green spectrum), and 1000 nm (magenta spectrum) monitoring the charge separation and charge recombination.*

Conclusions

The versatility of newly synthesized carbon nanodots (pCND) featuring unique electron-donating ability and negatively charged edge groups was explored in self assembling electron donor-acceptor hybrids. pCNDs were combined with electron-accepting and positively charged perylenediimides (PDI) **1**, by virtue of ionic and π-π interactions to afford pCND/**1**. The binding constants are as high as 8 $\times 10^4$ M^{-1} and/or 25 L g^{-1}. For pCND/**1**, corroboration of ionic interactions between the carboxylate and ammonium groups, on the one hand, and for π-π interactions on the other, came from Density-Functional Theory calculations. In reference experiments, in which negatively charged perylenediimides (PDI) **2** were tested, pCNDs fail to reveal any notable changes. Moreover, we infer sizeable charge shift from the pCNDs to **1** in the ground state from configuration-interaction calculations. In the excited state of pCND/**1**, which was probed by steady state/time resolved fluorescence spectroscopy and femtosecond transient-absorption spectroscopy, PDI fluorescence quenching results in charge separation to afford the one-electron oxidized pCND and the one-electron reduced **1**. The charge separated state lifetime in pCND/**1** is 210 ps.

Experimental Section

The synthetic procedure of pCNDs followed our mild microwave synthesis protocol. Urea and citric acid were mixed in a molar ratio of 3:1 and reacted in a microwave reactor at 150°C and 15 bar for 5 min. The product was precipitated in acetone to remove excess of the precursors. Then the product was washed in MeOH several times. In the last step, the solvent was evaporated at 70°C. The remaining solid was used for further analysis. PDI **1** was synthesized in the Group of Maurizio Prato and published elsewhere. PDI **2** was synthesized in the Group of Andreas Hirsch and published elsewhere. [32] Fluorescence quantum yields were determined in H_2O by the gradient method against Sulforhodamin B as a reference.

Steady-state Absorption measurements were carried out with a Lambda 2 UV/Vis/NIR-spectrometer (Perkin Elmer) or a Cary 5000 UV/Vis/NIR-spectrometer (Varian). Steady-state fluorescence emission

measurements were performed with a FluoroMax®-3 (Horiba). Time-correlated single-photon counting was perfomed with a FluoroLog®-3 spectro-fluorometer (Horiba). All spectra were corrected for the instrument response. Femtosecond transient-absorption studies were carried out using a transient absorption pump/probe system (Clark-MXR Inc.) connected to a CPA-2101 laser. 0.05 M phosphate buffer solutions in D_2O were used for all spectroscopic measurements unless otherwise noted.
Voltammetric measurements were performed with a three-electrode setup using a 3 mm glassy carbon disk as working electrode, a platinum wire as counter-electrode, and Ag/AgCl reference electrode. The solutions were thoroughly deoxygenated prior to the measurements.

Literature

(1) Jariwala, D.; Sangwan, V. K.; Lauhon, L. J.; Marks, T. J.; Hersam, M. C. *Chem. Soc. Rev.* **2013**, *42*, 2824–60.

(2) Torres, T.; Bottari, G. *Organic Nanomaterials*; Wiley, 2013.

(3) Balzani, V.; Credi, A.; Venturi, M. *Molecular devices and machines: concepts and perspectives for the nanoworld*; Wiley-VCH, 2008.

(4) Falcao, E. H. L.; Wudl, F. *J. Chem. Technol. Biotechnol.* **2007**, *531*, 524–531.

(5) Akasaka, T.; Fred, W.; Nagasu, S. *Chemistry of Nanocarbons*; Akasaka, T.; Fred, W.; Nagasu, S., Eds.; Wiley, 2010.

(6) Pumera, M. *Energy & Environmental Science* **2011**, *4*, 668.

(7) Gao, C.; Guo, Z.; Liu, J.-H.; Huang, X.-J. *Nanoscale.* **2012**, *4*, 1948–63.

(8) Putzbach, W.; Ronkainen, N. J. *Sensors. Basel. Sensors.* **2013**, *13*, 4811–40.

(9) Dirian, K.; Herranz, M. Á.; Katsukis, G.; Malig, J.; Rodríguez-Pérez, L.; Romero-Nieto, C.; Strauss, V.; Martín, N.; Guldi, D. M. *Chemical Science* **2013**, *4*, 4335–4353.

(10) Guldi, D. M.; Costa, R. D. **2013**.

(11) Isla, H.; Grimm, B.; Pérez, E. M.; Rosario Torres, M.; Ángeles Herranz, M.; Viruela, R.; Aragó, J.; Ortí, E.; M. Guldi, D.; Martín, N. *Chemical Science* **2012**, *3*, 498.

(12) Grimm, B.; Schornbaum, J.; Jasch, H.; Trukhina, O.; Wessendorf, F.; Hirsch, A.; Torres, T.; Guldi, D. M. *Proc. Natl. Acad. Sci. US. A.* **2012**, *109*, 15565–71.

(13) Nielsen, K. a.; Martín-Gomis, L.; Sarova, G. H.; Sanguinet, L.; Gross, D. E.; Fernández-Lázaro, F.; Stein, P. C.; Levillain, E.; Sessler, J. L.; Guldi, D. M.; Sastre-Santos, Á.; Jeppesen, J. O. *Tetrahedron.* **2008**, *64*, 8449–8463.

(14) Nielsen, K. a; Cho, W.-S.; Sarova, G. H.; Petersen, B. M.; Bond, A. D.; Becher, J.; Jensen, F.; Guldi, D. M.; Sessler, J. L.; Jeppesen, J. O. *Angew. Chem. Int. Ed. Engl.* **2006**, *45*, 6848–53.

(15) Do, S.; Kwon, W.; Rhee, S.-W. *Journal of Materials Chemistry C* **2014**, *2*, 4221.

(16) Margraf, J. T.; Strauss, V.; Guldi, D. M.; Clark, T. *Journal of Physical Chemistry C* **2015**.

(17) Tang, L.; Ji, R.; Cao, X.; Lin, J.; Jiang, H.; Li, X.; Teng, K. S.; Luk, C. M.; Zeng, S.; Hao, J.; Lau, S. P. *ACS. Nano.* **2012**, *6*, 5102–5110.

(18) Ming, H.; Ma, Z.; Liu, Y.; Pan, K.; Yu, H.; Wang, F.; Kang, Z. *Dalton. Trans.* **2012**, *41*, 9526–31.

(19) Lu, J.; Yeo, P. S. E.; Gan, C. K.; Wu, P.; Loh, K. P. *Nat. Nanotechnol.* **2011**, *6*, 247–52.

(20) Li, H.; Kang, Z.; Liu, Y.; Lee, S.-T. *J. Mater. Chem.* **2012**, *22*, 24230–24253.

(21) Ghosh, S.; Chizhik, A. M.; Karedla, N.; Dekaliuk, M. O.; Gregor, I.; Schuhmann, H.; Seibt, M.; Bodensiek, K.; Schaap, I. A. T.; Schulz, O.; Demchenko, A. P.; Enderlein, J.; Chizhik, A. I. *Nano Lett* **2014**.

(22) Strauss, V.; Margraf, J. T.; Dolle, C.; Butz, B.; Nacken, T. J.; Walter, J.; Bauer, W.; Peukert, W.; Spiecker, E.; Clark, T.; Guldi, D. M. *J. Am. Chem. Soc.* **2014**, *136*, 17308–16.

(23) Yu, P.; Wen, X.; Toh, Y.-R.; Lee, Y.-C.; Huang, K.-Y.; Huang, S.; Shrestha, S.; Conibeer, G.; Tang, J. *Journal of Materials Chemistry C* **2014**, *2*, 2894.

(24) Kwon, W.; Lee, G.; Do, S.; Joo, T.; Rhee, S.-W. *Small.* **2014**, *10*, 506–13.

(25) Xu, X.; Ray, R.; Gu, Y.; Ploehn, H. J.; Gearheart, L.; Raker, K.; Scrivens, W. A. *J. Am. Chem. Soc.* **2004**, *126*, 12736–7.

(26) Song, Y.; Zhu, S.; Xiang, S.; Zhao, X.; Zhang, J.; Zhang, H.; Fu, Y.; Yang, B. *Nanoscale.* **2014**, *6*, 4676–82.

(27) Strauss, V.; Margraf, J. T.; Clark, T.; Guldi, D. M. *J. Am. Chem. Soc.* **2015**.

(28) Oelsner, C.; Schmidt, C.; Hauke, F.; Prato, M.; Hirsch, A.; Guldi, D. M. *J. Am. Chem. Soc.* **2011**, *133*, 4580–6.

(29) Iron, M. A.; Cohen, R.; Rybtchinski, B.; It, A.; Phys, J. *The Journal of Physical Chemistry A* **2011**, *115*, 2047–2056.

(30) Nagao, Y. *Prog. Org. Coat.* **1997**, *2*, 43–49.

(31) Chen, L.; Li, C.; Müllen, K. *Journal of Materials Chemistry C* **2014**, *2*, 1938.

(32) Schmidt, C. D.; Böttcher, C.; Hirsch, A. *Eur. J. Org. Chem.* **2007**, 5497–5505.

(33) Würthner, F.; Chen, Z.; Dehm, V.; Stepanenko, V. *Chem. Commun. (Camb).* **2006**, *4*, 1188–90.

(34) Qu, S.; Wang, X.; Lu, Q.; Liu, X.; Wang, L. *Angew. Chem. Int. Ed. Engl.* **2012**, *51*, 12215–8.

(35) Ehli, C.; Oelsner, C.; Guldi, D. M.; Mateo-alonso, A.; Prato, M.; Schmidt, C.; Backes, C.; Hauke, F.; Hirsch, A. *Nature Chemistry* **2009**, *1*, 243–249.